Journal of Materials Chemistry A

Accepted Manuscript

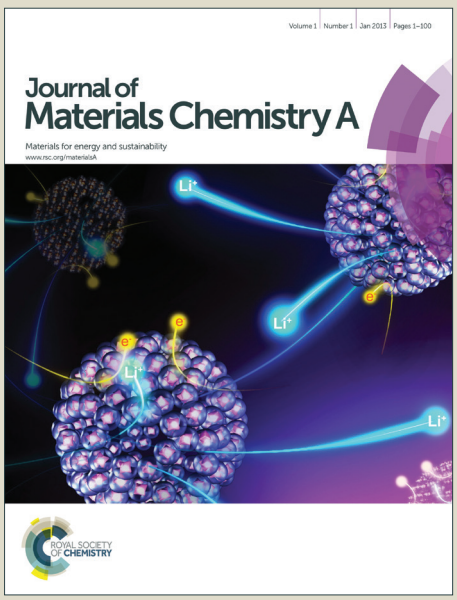

ROYAL SOCIETY OF CHEMISTRY

www.rsc.org/materialsA

NiS Nanorods-assembled Nanoflower Grown on Graphene: Morphology Evolution and Li-ion Storage Application

Hua Geng, Shao Feng Kong, Yong Wang*

Department of Chemical Engineering, School of Environmental and Chemical Engineering, Shanghai University , Shangda Road 99, Shanghai, 200444, P. R. China.

Email: yongwang@shu.edu.cn

Abstract

This paper reports morphology, size and phase control of NiS nanoflowers on graphene substrate. The growth mechanism for various building blocks for NiS nanoflower such as nanosheet, nanoflake, and nanorod is explored under varied experimental conditions. All obtained NiS nanoflowers are found to be uniformly dispersed on graphene nanosheets, forming a sandwiched nanostructure. When fabricated as an anode material for Li-ion batteries, graphene supported NiS nanorod-assembled nanoflower shows better cycling performances than pristine NiS and other NiS-graphene composites. It shows a large unprecedented reversible lithium-extraction capacity of 887 mAh g^{-1} after 60 cycles at 59 mA g^{-1} and good high-rate capability among NiS-based anodes.

Keywords: Flower-on-sheet, Graphene, Li-ion Batteries, Nanorod, NiS.

Introduction

Lithium-ion batteries are widely used for portable devices because of their large energy density, long cycle life and high operation voltage. Metal sulfides such as NiS, CoS, SnS_2 and MoS_2 have attracted significant research interest as anodes for Li-ion batteries basically because their theoretical capacities are substantially larger than that of commercial graphite (372 mAh g^{-1}).[1-12] For example, as an anode for Li-ion batteries, NiS has a high theoretical capacity of 590 mAh g^{-1}.[1-7] However, these metal sulfides usually display poor cycling stabilities, which has been mainly attributed to the large volume change during repetitive cycling. An effective strategy is to use various carbonaceous materials to support these anodes such as NiS.[13-17] This is because most carbons are flexible, robust, and conductive and they can greatly buffer the volume change of the supported NiS and increase its electronic conductivity and mechanical stability. Moreover carbon by itself is also an active anode to store Li-ions. As a popular carbon, graphene nanosheet has been demonstrated as such a matrix to be composited with various high-capacity anodes.[8-13]

Various NiS-based materials have been prepared and applied with important energy applications such as Li-ion batteries, supercapacitors and solar cells.[13-29] Its high electronic conductivity and low cost are also favorable for energy storage in electric vehicles. Few studies have been reported on the synthesis of NiS-graphene composites in which two NiS morphologies on graphene: particle-on-sheet,[23,24,29] and

sheet-on-sheet[13,28] were reported. With respect to Li-ion storage application, the only report comes from the NiS-graphene sheet-on-sheet nanostructure,[13] which shows substantially improved Li-ion storage properties than other NiS anodes.

In this study, NiS sheet-assembled nanoflower and its morphology evolution are explored. NiS nanoflake/nanorod-assembled nanoflowers can be obtained with size control by varying the usage amount of graphene nanosheets in the preparation process. Graphene supported NiS flower consisting of nanorods showed large Li-ion storage capacities at both small and large current densities as well as good cycling stabilities.

Experimental

Materials Preparation

Preparation of NiS-graphene composites: Graphene nanosheets (GNS) were synthesized by a modified Hummers method followed by thermal reduction as reported elsewhere previously.[10] In a typical synthesis of NiS-graphene composites: 0.2 g nickel chloride hexhydrate (Sinopharm Chemical) and 0.128 g thiourea (Sinopharm Chemical) were dissolved in 10 ml ethanol (Sinopharm Chemical) to form a transparent solution. A calculated amount of GNS was ultrasonically dispersed in 10 ml ethanol for 2h and then mixed with the above solution. 0.076, 0.038, 0.025 or 0.019 g GNS were used to form NiS-GNS composites with weight ratios of NiS to GNS: 1:1, 2:1, 3:1, and 4:1 respectively. The mixture suspension was stirred for 2 h and then sealed in a 60 ml

Teflon lined stainless steel autoclave for a solvothermal reaction at 180 ^{o}C for 12 h. The resulting black powders were collected after centrifuging, washed several times, and then dried at 60 ^{o}C for 24 h.

Pristine NiS nanoflowers consisting of nanosheets were prepared under the same conditions in the absence of GNS except that 20 ml ethanol was used to dissolve nickel chloride hexhydrate and thiourea.

Materials Characterization

The samples were characterized by X-ray diffraction (XRD, Rigaku D/max-2550V, Cu Kα radiation), field-emission scanning electron microscopy (FE-SEM, JSM-6700F) with an energy dispersive X-ray spectrometer (EDS), and transmission electron microscopy (TEM, JEOL JEM-200CX and JEM-2010F) in the Instrumental Analysis and Research Center, Shanghai University. Raman spectroscopy was recorded on Renishaw in plus laser Raman spectrometer (excitation wavelength: 785 nm, excitation power: 3 mW, spot size: ~1.2 μm). The electrical conductivity was measured by a four-electrode method using a conductivity detection meter (Shanghai Fortune Instrument, FZ-2010). BET surface areas and pore size were determined by gas sorption technique on Micromeritics' ASAP 2020. The carbon and sulphur elements were measured by an elemental analyzer (Vario Micro).

Electrochemical Measurement

Electrochemical Li storage performances of samples were evaluated in Swagelok-type Laboratory half cells. The specific capacities of NiS-graphene composites were obtained based on the total mass of the composite. The working electrodes were consist of 80 wt% of active material, 10 wt% of acetylene black and 10 wt% of the poly(vinylidene fluoride)(PVDF) binder, using N-methy1-2 -pyrrolidinone (NMP) as a dispersant to form a slurry. Lithium foil (China Energy Lithium) was used as counter and reference electrode. The electrolyte was 1M $LiPF_6$ in a 1:1 w/w mixture of ethylene carbonate (EC) and diethyl carbonate (DEC). The loading amount of active material on the current collector (Cu foil) was kept around 1.5 mg cm^{-2}. Cell assembly was carried out in a recirculating argon glove box where both the moisture and oxygen contents were below 1 ppm each. Electrochemical measurements were performed on a LAND-CT2001 test system. The Swagelok-type cells were discharged (lithium insertion) and charged (lithium extraction) at a constant current (59 mA g^{-1}, 0.1 C) in the fixed voltage range 5 mV– 3 V. Higher hourly rates (0.5, 1 and 2 C) were also used and the first cycle discharging was kept at 0.1 C. Cyclic voltammetry was performed on a CHI660D electrochemical workstation at a scan rate of 0.1 mV/s. Electrochemical impedance was performed on a CHI660D electrochemical workstation.

Results and Discussion

Figure 1 shows the XRD patterns of NiS and various NiS-graphene nanosheets(GNS) composites. Pristine NiS displays a few characteristic peaks with strong intensities,

which can be corresponded to (110) (300) (021) (131) planes. All these diffraction peaks can be easily indexed to the β-NiS (PDF 12-0041). However, the obtained NiS-GNS composites exhibit different α-NiS phase, indicating the important effect of GNS on the crystal growth process of NiS. This should be ascribed to the residual functionalities such as hydroxyl and carboxyl groups on the thermally-reduced GNS.[11] All the characteristic peaks can be ascribed to standard α-NiS (PDF 02-1280) in various NiS-GNS composites with different amounts of GNS. Notably, a small amount of sulfur is present in pristine NiS because a small characteristic peak of sulfur can be observed at 20.3^{o}. NiS-GNS composite (1:1) does not exhibit the peak of sulfur element. There is a hump peak for graphene in NiS-GNS (1:1) composite, which is not obvious in other NiS-GNS composites.

Figure 2 shows the SEM and TEM images of pristine NiS nanoflowers prepared in the absence of graphene. These NiS flower-like microspheres (~0.8-1.4 μm in size) are composed of numerous nanosheets-like NiS products. If the reaction is performed at a shortened time of 6 h, nanosheet-assembled microspheres can be also observed (Figure 3a-c) but with a substantially reduced size of ~0.6-1.2 μm. When the reaction time is prolonged to 24 h, the size of microspheres is increased to ~1.6-2 μm (Figure 3d-f). Notably those wrinkled area or porous spaces among NiS nanosheets are largely reduced compared to the products prepared after 6 and 12 h reactions because smooth surface of several NiS flower-like microspheres can be observed in Figure 3d-e. If the concentration of nickel chloride and thiourea is reduced by 50%

and other experimental conditions are kept same, the obtained NiS nanoflowers show a reduced sphere size of 0.5-1.1 μm (Figure S1a, Supporting Information). Larger sphere sizes (~1.3-1.8 μm) can be observed at a doubled concentration of nickel chloride. (Figure S1b, Supporting Information). L-cysteine was also used to replace thiourea in the preparation and it was found that only NiS nanoparticles can be obtained (Figure S2, Supporting Information).

Various amounts of graphene were added in the preparation of NiS-GNS composites. Figure 4 shows SEM images of NiS-GNS composites with different weight ratios of NiS to GNS (4:1, 3:1, 2:1). The presence of graphene has an important effect on the product morphology of NiS, but the sizes of NiS nanoflowers are roughly in the same range of 0.8-1.2 μm. Nanoflake-assembled NiS nanoflowers (Figure 4a-b) are observed in the NiS-GNS composite (4:1). With the increase of graphene, the individual building block intends to change from nanoflake to nanorod in the NiS-graphene composites (4:1, 3:1, 2:1) (Figure 4a-b, c-d, e-f respectively). It is indicated that the functionalities retained on graphene surface such as -OH, -COOH may affect the crystal growth of NiS by the possible –SH group linkage. The morphology evolution of NiS can be confirmed by the corresponding TEM images of NiS-GNS composites in Figure S3, Supporting Information. Moreover, the size change of NiS is not substantial compared to large morphology change as indicated by these TEM images.

If a large amount of graphene is used to form NiS-graphene composite (1:1), NiS nanorod-assembled nanoflowers are obtained as the main product of this work (Figure 5). These NiS spheres are around 0.8-1.2 μm in size and they are composed of sharp NiS nanorods with diameters at 30-40 nm. Compared to pristine NiS in the absence of graphene, the sphere size is slightly reduced, but the morphology of NiS building block is changed substantially from sheet-like morphology to nanorod-like morphology. It is also noted that several NiS nanoflowers are wrapped between two neighboring layers of graphene nanosheets as indicated by SEM images of Figure 5a-b. Therefore GNS are also separated by NiS nanoflowers and their agglomeration is prevented to some extents. The energy dispersive spectroscopy (EDS) of NiS-GNS flower-on-sheet composite is shown in Figure S4, Supporting Information. Several elements such as C, Ni, and S are present in the composite. The elemental mapping images of NiS-graphene composite are shown in Figure 6. Three elements (C, Ni, and S) are quite uniformly dispersed in the composite. Figure 7 shows TEM images of NiS-GNS composite (1:1). The obtained NiS nanoflowers are distributed uniformly on graphene surface. Individual NiS nanorods are clearly observed with diameters of 30-40 nm.

Based on the SEM and TEM observations of a series of NiS and NiS-graphene composites, the growth process of NiS nanoflower in the presence of graphene nanosheets(GNS) are summarized in Figure 8. In the absence of graphene, nanosheet-assembled NiS nanoflowers are obtained. If GNS are present in the

preparation of NiS-graphene composites, they would affect the crystal growth process of NiS by a possible linkage of thiol bonds between the surface group of GNS and NiS. It is demonstrated that there is still a small amount of carboxyl and hydroxyl groups confirmed by XPS on the surface of the thermally-reduced GNS in our previous publication.[11] Figure 8 shows that morphology evolution of NiS products can be observed in the composites with the increased usage amounts of GNS. NiS displays a nanoflake-like morphology in NiS-graphene (4:1) and changes to nanorod-assembled flower morphology in NiS-graphene (3:1). The NiS nanorod tends to be sharper with further increased amounts of graphene in NiS-graphene composites (2:1 and 1:1). Raman spectra of GNS and NiS-GNS composite (1:1) is shown in Figure S5a, Supporting Information. The intensity ratio (I_D: I_G) of the D band (located at 1330 cm^{-1}) to G band (located at 1590 cm^{-1}) for bare graphene is 1.18, which is smaller than NiS-GNS composite (1.41). The more disordered carbon structure in NiS-GNS implies that there are more defects generated on GNS. This is possibly ascribed to the insertion of some NiS into graphene layers because the $NiCl_2$ precursor may be inserted into graphene layers and form NiS there. Similar intercalation phenomenon has been reported previously[30-31]. These defects may be used to store extra amount of lithium ions and facilitate the lithium diffusion and electrolyte soakage.[10,12] The Brunauer-Emmett-Teller (BET) analysis of NiS-GNS composite with the nitrogen adsorption-desorption isotherm is shown in Figure S5b, Supporting Information. The BET surface area of NiS-GNS was measured to be 87.6 m^2 g^{-1}. These pores are estimated to be ~3.2 nm based on the BJH analysis, the inset

of Figure S5b. Elemental analysis reveals that the carbon contents are 24.78%, 28.3%, 35.76%, and 57.36% in graphene-NiS composites with weight ratios (graphene versus NiS) of 1:4, 1:3, 1:2, and 1:1 respectively.

Figure 9 shows the electrochemical performances of pristine NiS and NiS-GNS composites (1:1 and 2:1) between 5 mV and 3 V at 59 mA g^{-1} (0.1 C). The first, second and 60th cycles of discharge (lithium insertion) and charge (lithium extraction) curves of pristine NiS and NiS-GNS composite (1:1) are shown in Figure 9a and 9b respectively. There are two obvious voltage plateaus (~1.72 and 1.27 V) in the discharge curve of NiS anode. These two plateaus can be attributed to the following two stepwise reactions. NiS reacts with lithium to form intermediate products of Ni_3S_2 and Li_2S at the first stage and then form Ni and Li_2S at the second stage. There are also two plateaus ~2.03 V and 2.22 V in the charge curve, corresponding to the reversible two reactions from Ni to NiS. These reversible electrochemical reactions between NiS and lithium can be described by the following two equations:

$$3NiS+2Li \longleftrightarrow Ni_3S_2+Li_2S$$

$$Ni_3S_2+4Li \longleftrightarrow 3Ni+2Li_2S$$

Cyclic voltammery (CV) curves of the NiS/GNS composites was recorded at a scan rate of 0.1 mV s^{-1} between 5 mV and 3 V (Figure S6, Supporting Information). There are two cathodic peaks at around 1.21 V and 1.72 V and two anodic peaks at around 2.05 V and 2.20 V, which agree well with previous discharge and charge curves of NiS anodes.

The cycling performances of various products are compared in Figure 9c. It is obvious that the cycling performances of NiS-GNS (1:1) are better than pristine NiS, bare graphene and NiS-GNS (2:1). The first discharge and charge capacities are 985/660 and 1977/905 mAh g^{-1} respectively for pristine NiS and bare graphene. These values are increased to 1774 and 976 mAh g^{-1} for NiS-GNS composite(1:1). The high reversible charge capacity of the composite may be mainly ascribed to the contribution of disordered graphene. Extra amount of lithium have been suggested to be stored in pores or defects of the disordered graphene structure in the graphene-based anodes.[9-11] An extremely large reversible capacity of ~1054 mAh g^{-1} was also reported for disordered garphene.[32] The more disordered graphene structure in the composite compared to bare graphene has been confirmed by the Raman spectra (Figure S5a, Supporting Information) in this work. The first-cycle irreversible capacity loss should be largely due to the formation of solid electrolyte interface (SEI) film on the surface of NiS-GNS composite electrode. After 60 cycles, NiS-GNS (1:1) still exhibits a large reversible charge capacity of 887 mAh g^{-1}, while only a small reversible capacity of 144 or 458 mAh g^{-1} was retained for pristine NiS and NiS-GNS (2:1) respectively. The capacity fading is calculated to be 0.15% per cycle for NiS-GNS composite (1:1). The improvement of electrochemical properties can be mainly ascribed to the presence of graphene. Graphene is flexible, robust, highly-conductive, therefore the volume change with NiS anode can be largely buffered and its electrical conductivity can be also improved.[9-13] On the other hand,

the presence of metal sulfides can be also regarded as a spacer to prevent the restacking of GNS to graphite platelets, therefore unique properties relative to few-layer graphene can be largely maintained during cycling with lithium. Therefore a synergetic effect can be observed in the NiS-GNS composites. Notably, this large reversible capacity (887 mAh g^{-1} after 60 cycles) has not been witnessed in previous various carbonaceous materials supported NiS composites[13-17].

High-rate performances of NiS-GNS (1:1) are shown in Figure 10 and Figure S7, Supporting Information, at various currents of 0.5, 1 and 2 C (1 C=590 mA g^{-1}). The initial charge capacities of NiS-GNS are 941, 884, and 867 mAh g^{-1} at 295 mA g^{-1} (0.5 C), 590 mA g^{-1} (1 C), and 1180 mA g^{-1} (2 C) respectively. The NiS-GNS composite also exhibits good cycling performances at high current rates. The reversible charge capacities of composites can still be retained at 500, 383, and 298 mAh g^{-1} at 0.5, 1, and 2 C respectively after 100 cycles. Figure S8 in Supporting Information shows the Nyquist plots of pristine NiS and NiS-GNS at 59 mA g^{-1} after 5 cycles. The Nyquist plots consist of a depressed semicircle and a sloping line. The semicircle in the high frequency region is corresponded to the SEI film resistance (R_f) and the middle frequency region corresponds to the charge transfer impedance (R_{ct}). R_f and R_{ct} of pristine NiS are 90.5 Ω and 82.4 Ω and these values are substantially reduced for NiS-GNS composite (R_f = 43.9 Ω and R_{ct} =55.1 Ω). The electrical conductivities of NiS and NiS-GNS electrodes were also measured by a four-electrode method. The electrical conductivity of NiS is 0.058 S cm^{-1}, which is increased to

0.166 S cm^{-1} for NiS-GNS composite. It is indicated that the presence of GNS can facilitate the lithium diffusion in NiS-GNS composite compared to pristine NiS.

Conclusion

In summary, graphene supported NiS nanoflowers were obtained successfully in this work. The presence of graphene has an important effect on the product morphology, size and crystal phase of NiS nanoflower. The building blocks for NiS nanoflowers could be tuned from nanoflake, to mixed nanoflake-nanorod, then to sharp nanorod with the increased amount of GNS in NiS-GNS composites. When used as anodes for Li-ion batteries, NiS nanorod-assembled nanoflowers grown on graphene (1:1) showed better cycling performances than pristine NiS and NiS-GNS composite (2:1). It showed a high reversible capacity of 887 mAh g^{-1} after 60 cycles at the current of 59 mA g^{-1} and good high-rate capabilities. The improved Li-ion storage properties have been ascribed to the synergetic effect between NiS and graphene, where enhanced electrical contact, electrode structure stability, reduced Li-ion diffusion pathway, and prevented graphene's agglomeration could be preserved during repetitive cycling.

Acknowledgements

The authors gratefully acknowledge the follow-up Program for Professor of Special Appointment in Shanghai (Eastern Scholar), the National Natural Science Foundation of China (51271105), Shanghai Municipal Government (11JC1403900, 11SG38,) and Innovative Research Team (IRT13078) for financial support. The authors also thank

Lab for Microstructure, Instrumental Analysis and Research Center, Shanghai University, for materials characterizations.

Supporting Information Available:

SEM (Fig. S1) and TEM (Fig. S2) images of NiS with varied precursor concentrations and sulfur sources. TEM images (Fig. S3) of NiS-graphene composites with various compositions. The EDS spectra (Fig. S4), Raman spectra and N_2 adsorption-desorption isotherm (Fig. S5) of NiS-GNS composite. The cyclic voltammograms results (Fig. S6) and the high-rate cycling performances (Fig. S7-8) of NiS-GNS composite.

References

1. S. C. Han, K. W. Kim, H. J. Ahn, J. H. Ahn and J. Y. Lee, *J. Alloy. Compd.* 2003, **361**, 247.

2. N. H. Idris, M. M. Rahman, S. L. Chou, J. Z. Wang, D. Wexler and H. K. Liu, *Electrochim. Acta* 2011, **58**, 456.

3. Y. Wang, Q. S. Zhu, L. Tao and X. W. Su, *J. Mater. Chem.* 2011, **21**, 9248.

4. L. W. Mi, Y. F. Chen, W. T. Wei, W. H. Chen, H. W. Hou and Z. Zheng, *RSC Adv.* 2013, **3**, 17431.

5. J. Z. Wang, S. L. Chou, S. Y. Chew, J. Z. Sun, M. Forsyth, D. R. Macfarlane and H. K. Liu, *Solid State Ionics* 2008, **179**, 2379.

6. J. Wang, S. Y. Chew, D. Wexler, G. X. Wang, S. H. Ng, S. Zhong and H. K. Liu, *Electrochem. Commun.* 2007, **9**, 1877.

7. K. Aso, H. Kitaura, A. Hayashi and M. Tatsumisago, *J. Mater. Chem*. 2011, **21**, 2987.

8. Y. Q. Zou and Y. Wang, *ACS Nano* 2011, **5**, 8108.

9. Y. Gu and Y. Wang, *RSC Adv.* 2014, **4**, 8582.

10. P. Chen, Y. Su, H. Liu and Y. Wang, *ACS Appl. Mater. Interfaces* 2013, **5**, 12073.

11. Y. Q. Zou and Y. Wang, *Nanoscale* 2011, **3**, 2615.

12. Y. Gu, Y. Xu and Y. Wang, *ACS Appl. Mater. Interfaces* 2013, **5**, 801.

13. Q. Pan, J. Xie, S. Y. Liu, G. S. Cao, T. J. Zhu and X. B. Zhao, *RSC Adv*. 2013, **3**,

3899.

14. K. Aso, A. Sakuda, A. Hayashi and M. Tatsumisago, *ACS Appl. Mater. Interfaces* 2013, **5**, 686.

15. M. Y. Son, J. H. Choi and Y. C. Kang, *J. Power Sources* 2014, **251**, 480.

16. K. Aso, A. Hayashi and M. Tatsumisago, *Electrochim. Acta* 2012, **83**, 448.

17. S. T. Sebastian, R. S. Jagan, R. Rajagoplan, A. Paravannoor, L. V. Menon, K. R. V. Subramanian and S. V. Nair, *RSC Adv*. 2014, **4**, 11673.

18. S. B. Ni, X. L. Yang and T. Li, *J. Mater. Chem.* 2012, **22**, 2395.

19. N. Mahmood, C. Z. Zhang and Y. L. Hou, *Small* 2013, **9**, 1321.

20. H. C. Ruan, Y. F. Li, H. Y. Qiu and M. D. Wei, *J. Alloy. Compd.* 2014, **588**, 357.

21. A. Ghezelbash, M. B. Sigman and B. A. Korgel, *Nano Lett.* 2004, **4**, 537.

22. W. B. Zhang, J. Li, X. H. Liu and B. Y. Tang, *Comp. Mater. Sci*. 2014, **83**, 412.

23. Z. C. Xing, Q. X. Chu, X. B. Ren, J. Q. Tian, A. M. Asiri, K. A. Alamry, A. O. Al-Youbi and X. P. Sun, *Electrochem. Commun.* 2013, **32**, 9.

24. A. M. Wang, H. L. Wang, S. Y. Zhang, C. J. Mao, J. M. Song, H. L. Niu, B. K. Jin and Y. P. Tian, *Appl. Surf. Sci.* 2013, **282**, 704.

25. L. R. Hou, C. Z. Yuan, D. K. Li, L. Yang, L. F. Shen, F. Zhang and X. G. Zhang, *Electrochim. Acta* 2011, **56**, 7454.

26. T. Zhu, Z. Y. Wang, S. J. Ding, J. S. Chen and X. W. Lou, *RSC Adv*. 2011, **1**, 397.

27. J. Q. Yang, X. C. Duan, Q. Qin and W. J. Zheng, *J. Mater. Chem. A* 2013, **1**, 7880.

28. Q. Pan, J. Xie, T. J. Zhu, G. S. Cao, X. B. Zhao and S. C. Zhang, *Inorg. Chem.* 2014, **53**, 3511.

29. H. Bi, W. Zhao, S. R. Sun, H. L. Cui, T. Q. Lin, F. Q. Huang, X. M. Xie and M. H. Jiang, *Carbon* 2013, **61**, 116.

30. T. H. Bointon, I. Khrapach, R. Yakimova, A. V. Shytov, M. F. Cracium and S. Russo, *Nano Lett.* 2014, **14**, 1751.

31. T. Lin, Y. Tang, Y. Wang, H. Bi, Z. Liu, F. Huang, X. Xie and M. Jiang, *Energy Environ. Sci.* 2013, **6**, 1283.

32. D. Pan, S. Wang, B. Zhao, M. Wu, H. Zhang, Y. Wang and Z. Jiao, *Chem. Mater.* 2009, **21**, 3136.

Figure Captions

Figure 1. XRD patterns of NiS and NiS-graphene nanosheets(GNS) composites.

Figure 2. (a-b) SEM and (c-d) TEM images of NiS nanosheet-assembled nanoflowers.

Figure 3. NiS nanoflowers prepared after different reaction time: (a-b) SEM images, 6 h, (c) TEM image, 6 h, (d-e) SEM images, 24 h, and (f) TEM image, 24 h.

Figure 4. TEM images of NiS/GNS composites with different mass ratios: (a-b) NiS:GNS=4:1, (c-d) NiS:GNS=3:1, and (e-f) NiS:GNS=2:1.

Figure 5. SEM images of NiS/GNS composite (1:1) at stepwise increased magnifications: (a) scale bar = 2μm, (b) scale bar = 1 μm, (c) scale bar = 200 nm, and (d) scale bar = 100 nm.

Figure 6. Elemental mapping images of NiS/GNS composite (1:1): (a) SEM image, (b) carbon element, (c) nickel element, and (d) sulphur element.

Figure 7. TEM images of NiS/GNS composite (1:1) at stepwise increased magnifications: (a) scale bar = 1 μm, (b-c) scale bar = 500 nm, and (d) scale bar = 200 nm.

Figure 8. Schematic illustration showing the morphology revolution of NiS in the presence of graphene nanosheets (GNS). The morphology of NiS changes from nanoflake to sharp nanorod-like morphology with the increased amounts of GNS in the preparation process.

Figure 9. Electrochemical performances: (a) discharge (lithium insertion) and charge (lithium extraction) curves of NiS, (b) discharge and charge curves of NiS : GNS (1:1), and (c) cycling performances of various products at 0.1C.

Figure 10. High-rate performances at 0.5-2 C: (a) discharge and charge curves, (b) cycling performances.

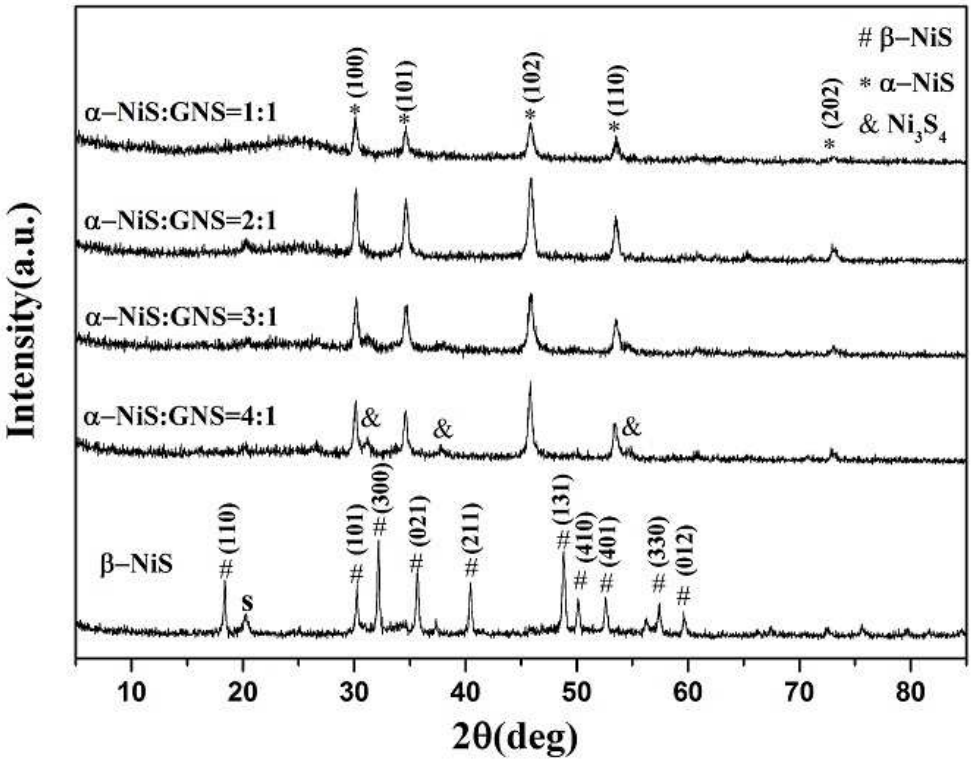

Figure 1. XRD patterns of NiS and NiS-graphene nanosheets(GNS) composites.

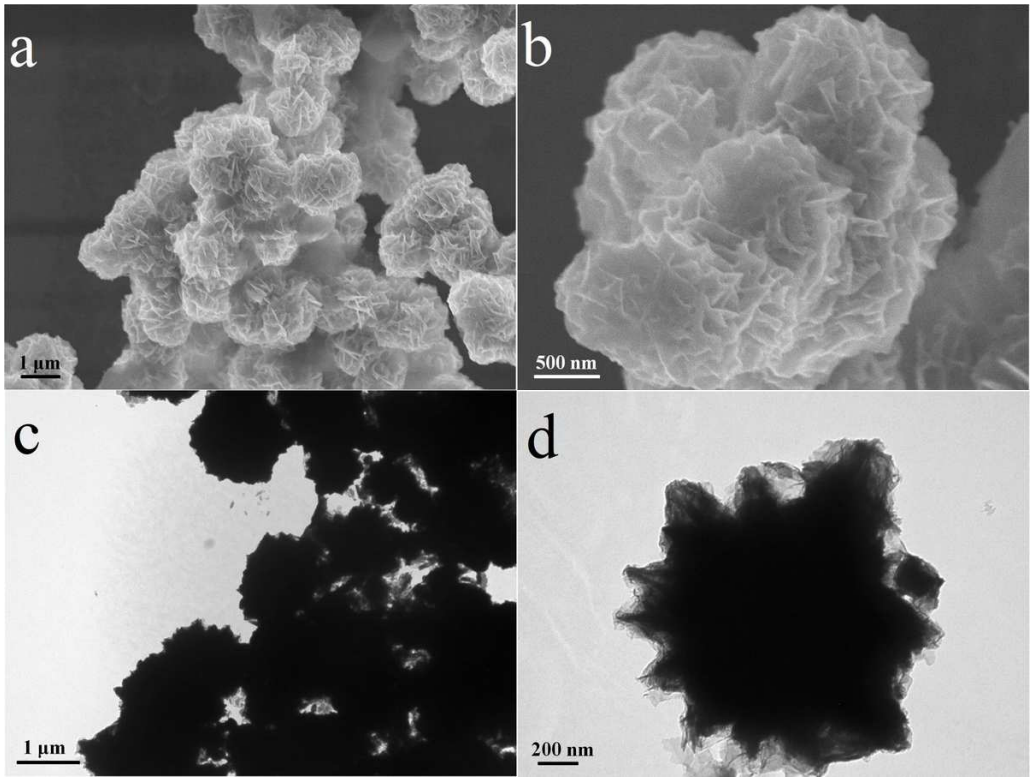

Figure 2. (a-b) SEM and (c-d) TEM images of NiS nanosheet-assembled nanoflowers.

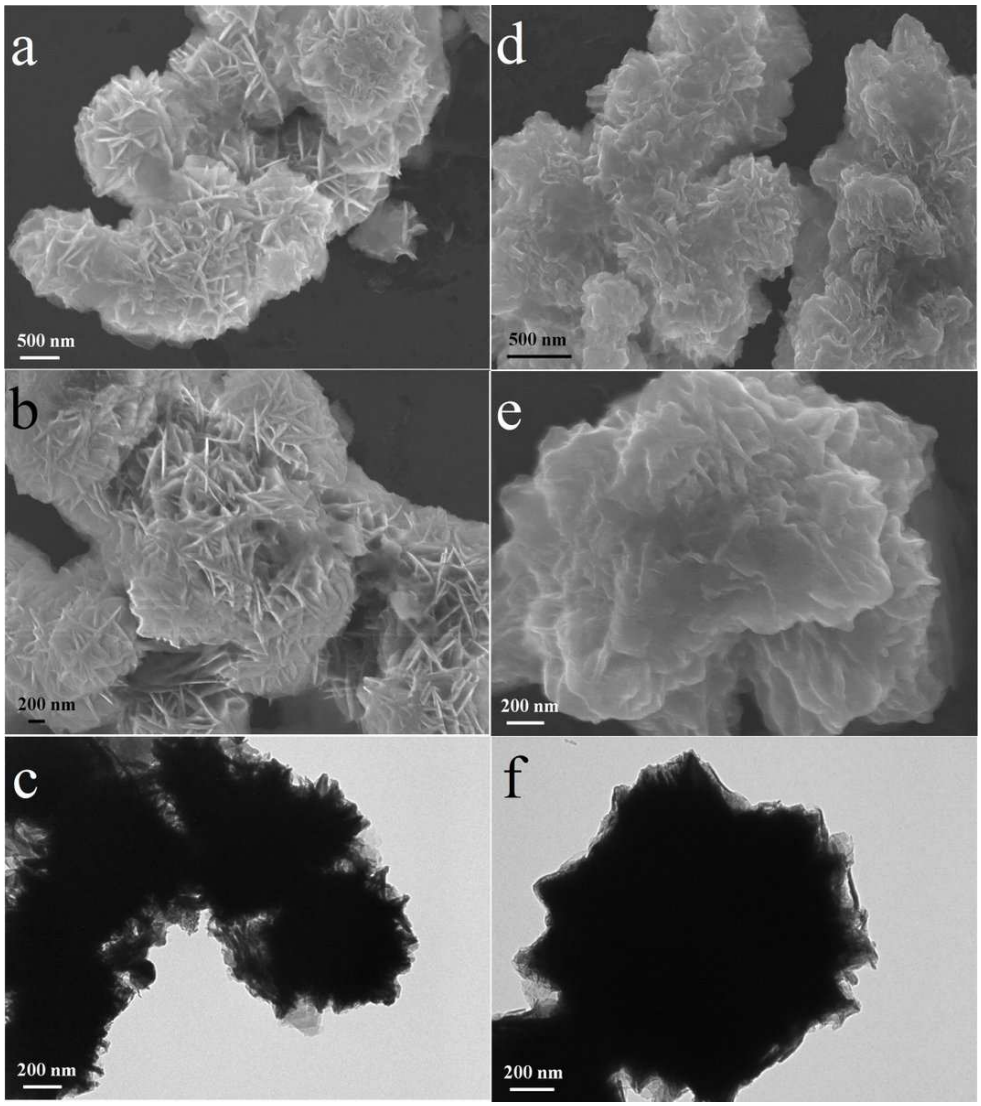

Figure 3. NiS nanoflowers prepared after different reaction time: (a-b) SEM images, 6 h, (c) TEM image, 6 h, (d-e) SEM images, 24 h, and (f) TEM image, 24 h.

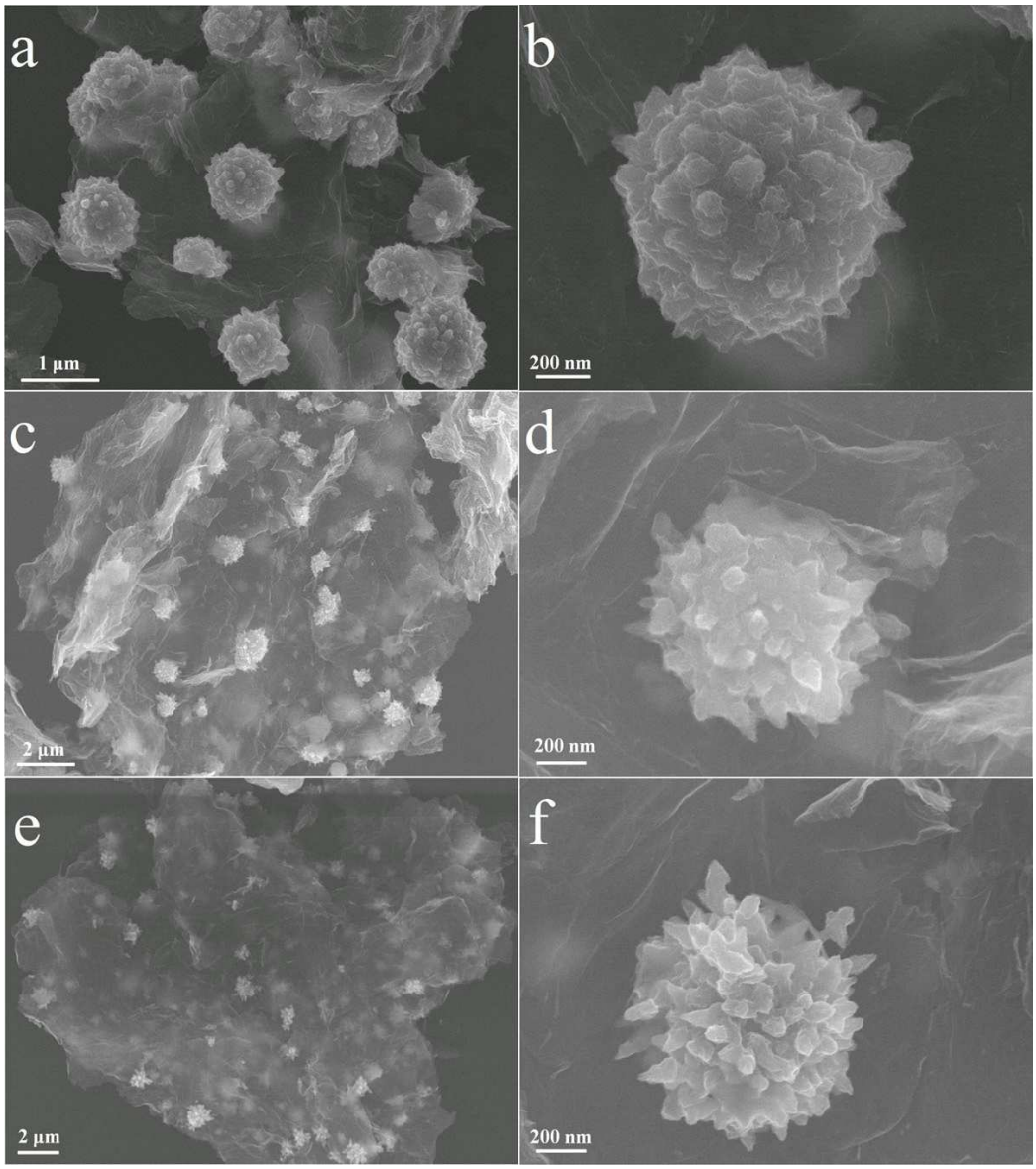

Figure 4. SEM images of NiS/GNS composites with different mass ratios: (a-b) NiS:GNS=4:1, (c-d) NiS:GNS=3:1, and (e-f) NiS:GNS=2:1.

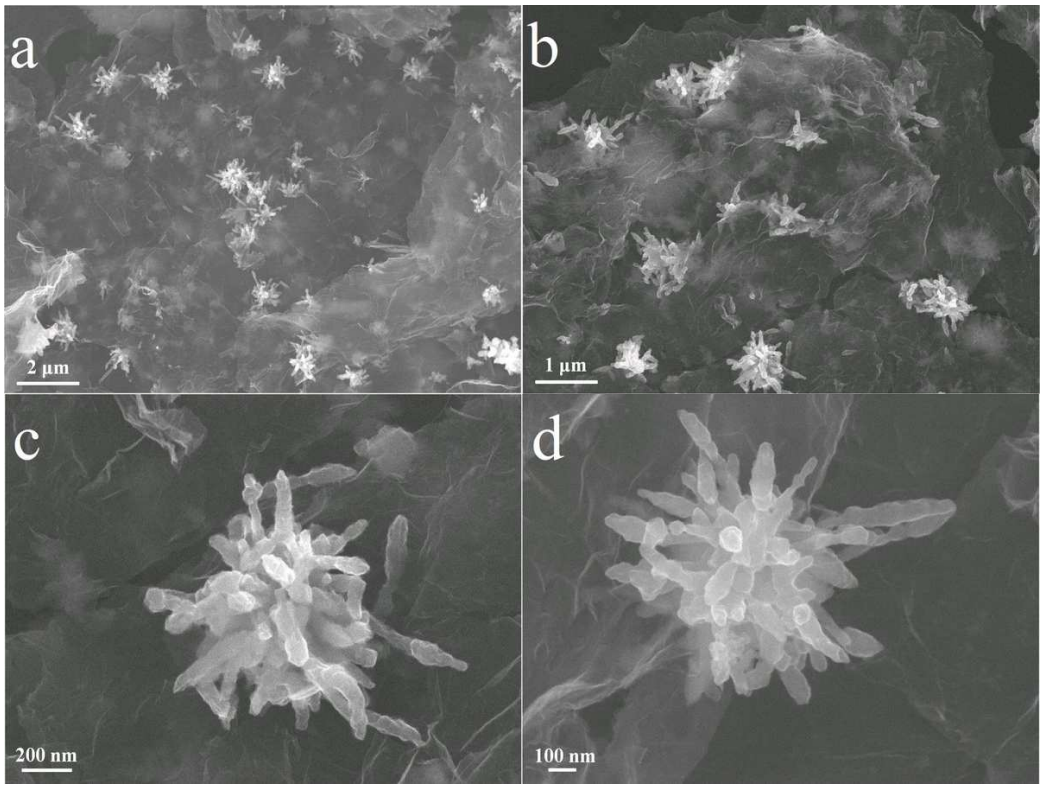

Figure 5. SEM images of NiS/GNS composite (1:1) at stepwise increased magnifications: (a) scale bar = 2μm, (b) scale bar = 1 μm, (c) scale bar = 200 nm, and (d) scale bar = 100 nm.

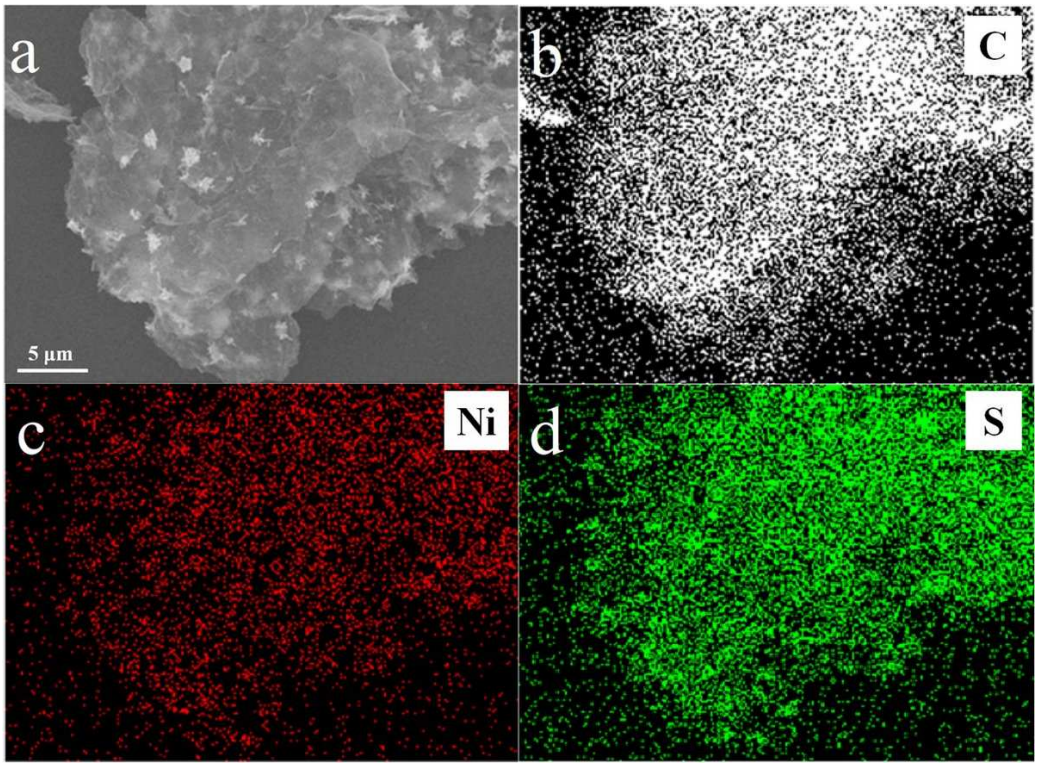

Figure 6. Elemental mapping images of NiS/GNS composite (1:1): (a) SEM image, (b) carbon element, (c) nickel element, and (d) sulphur element.

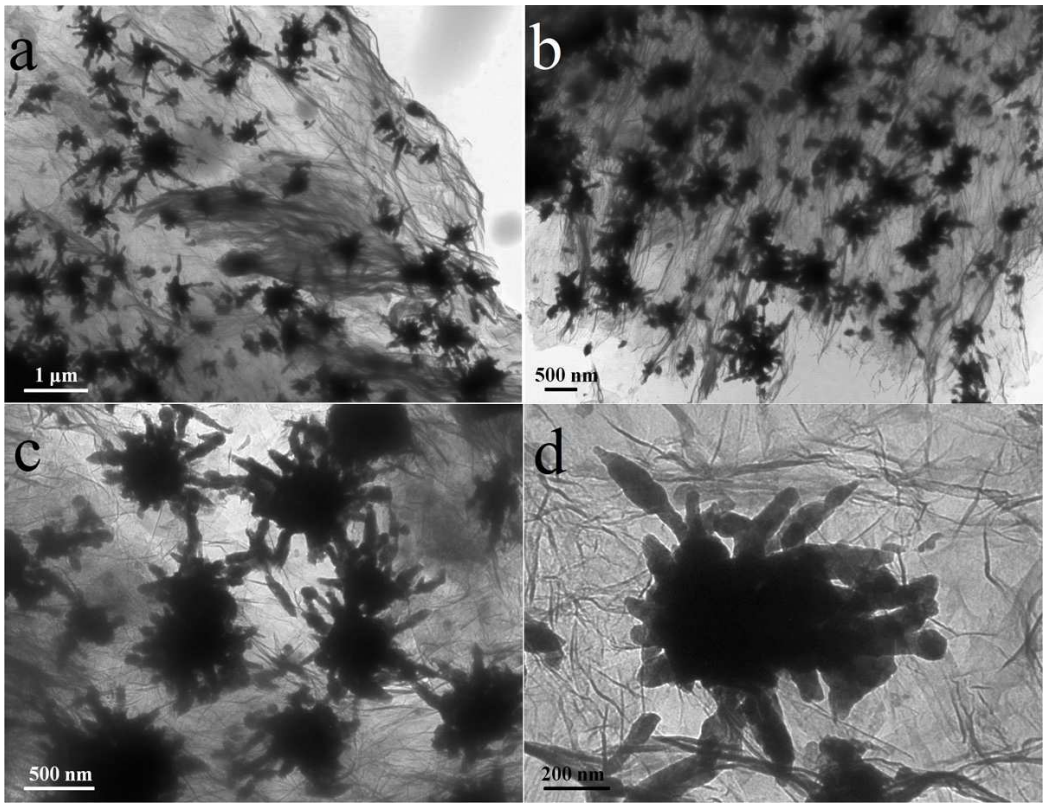

Figure 7. TEM images of NiS/GNS composite (1:1) at stepwise increased magnifications: (a) scale bar = 1 μm, (b-c) scale bar = 500 nm, and (d) scale bar = 200 nm.

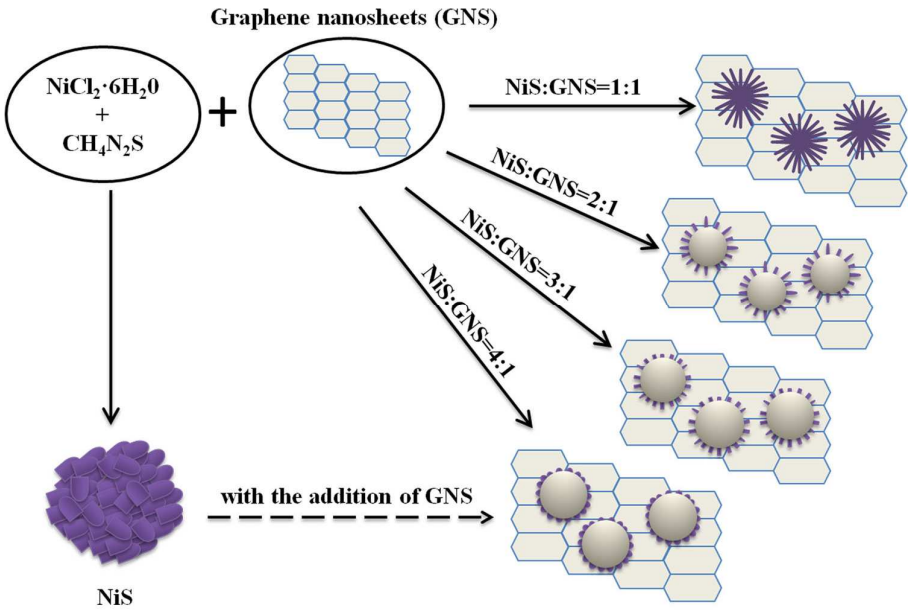

Figure 8. Schematic illustration showing the morphology revolution of NiS in the presence of graphene nanosheets (GNS). The morphology of NiS changes from nanoflake to sharp nanorod-like morphology with the increased amounts of GNS in the preparation process.

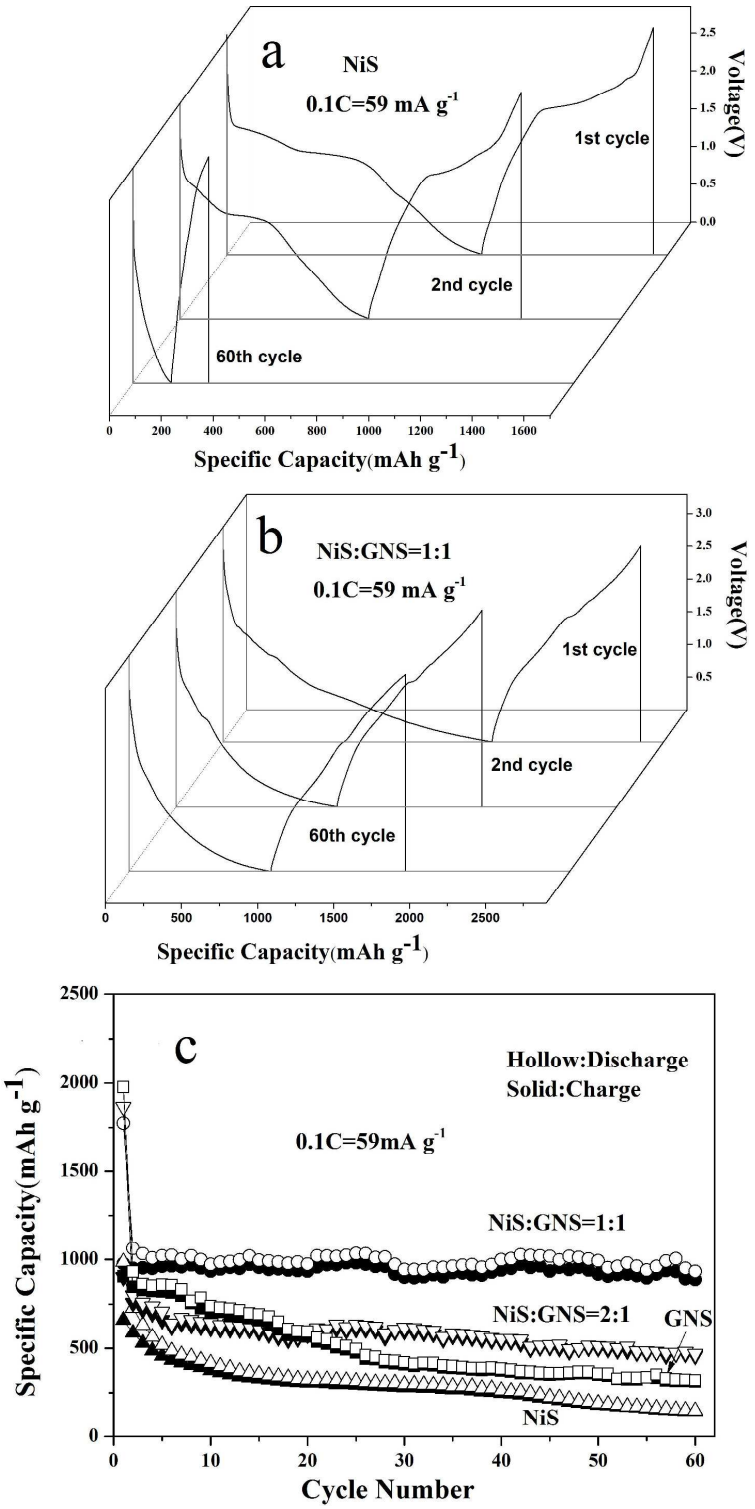

Figure 9. Electrochemical performances: (a) discharge (lithium insertion) and charge (lithium extraction) curves of NiS, (b) discharge and charge curves of NiS : GNS (1:1), and (c) cycling performances of various products at 0.1C.

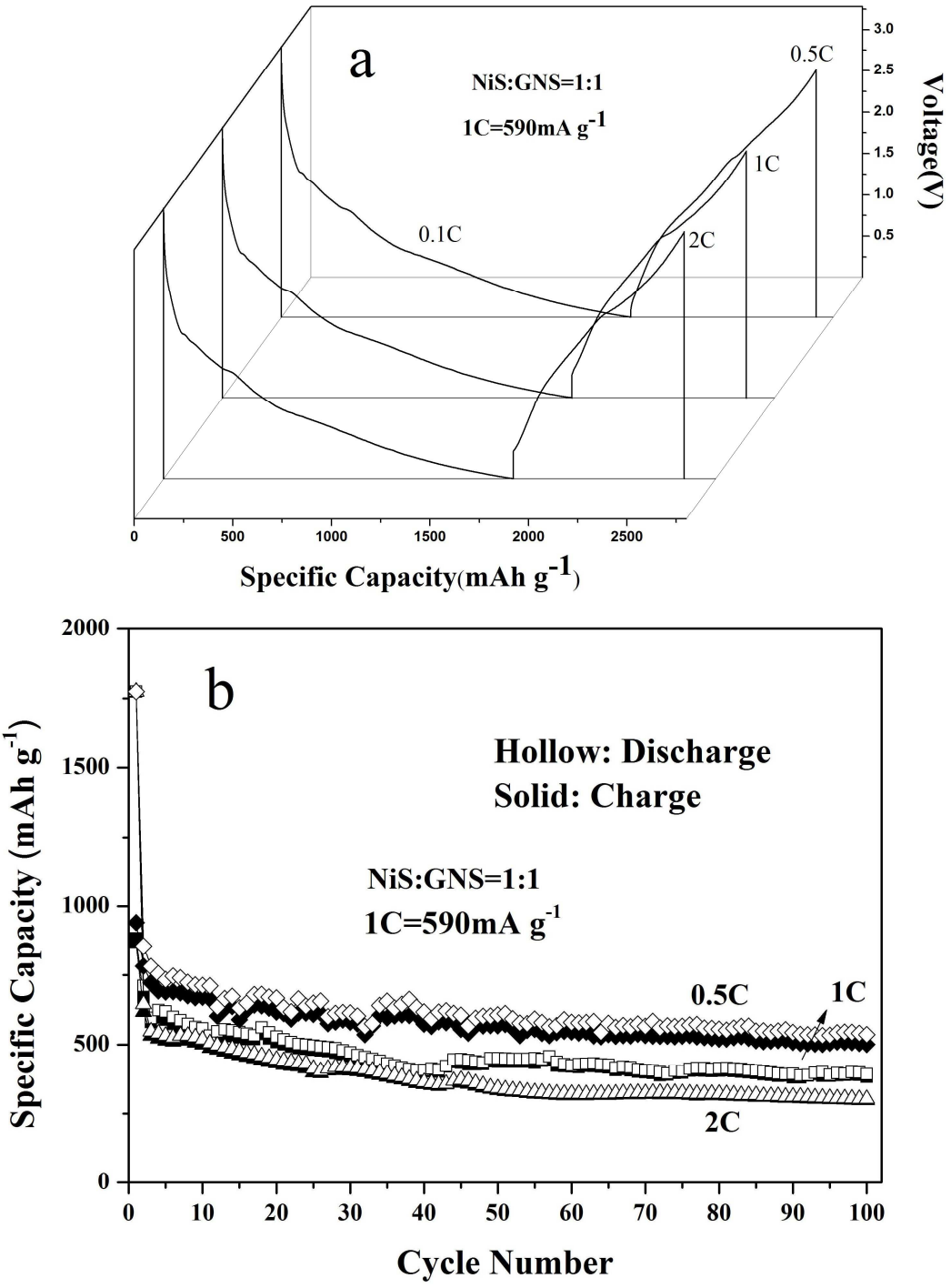

Figure 10. High-rate performances at 0.5-2 C: (a) discharge and charge curves, (b) cycling performances.

For Table of Contents

Morphology, size and phase of NiS nanoflowers are tuned in the preparation of NiS-graphene composite, which shows large reversible capacities at both small and high current rates for rechargeable Li-ion batteries.

Keywords: *Flower-on-sheet, Graphene, Li-ion Batteries, Nanorod, NiS.*

NiS Nanorods-Assembled Nanoflower Grown on Graphene: Morphology Evolution and Li-ion Storage Application

Hua Geng，Shao Feng Kong, Yong Wang*